Active Fluidification of Entangled Polymers by Loop Extrusion

Filippo Conforto,[1] Yair Augusto Gutierrez Fosado,[1] and Davide Michieletto[1,2]

[1]*School of Physics and Astronomy, University of Edinburgh, Peter Guthrie Tait Road, Edinburgh, EH9 3FD, UK*

[2]*MRC Human Genetics Unit, Institute of Genetics and Cancer, University of Edinburgh, Edinburgh EH4 2XU, UK*

Loop extrusion is one of the main processes shaping chromosome organisation across the cell cycle, yet its role in regulating DNA entanglement and nucleoplasm viscoelasticty remains overlooked. We simulate entangled solutions of linear polymers under the action of generic Loop Extruding Factors (LEF) with a model that fully accounts for topological constraints and LEF-DNA uncrossability. We discover that extrusion drives the formation of bottle-brush-like structures which significantly lower the entanglement and effective viscosity of the system through an active fluidification mechanism. Interestingly, this fluidification displays an optimum at one LEF every 300-3000 base-pairs. In marked contrast with entangled linear chains, the viscosity of extruded chains scales linearly with polymer length, yielding up to 1000-fold fluidification. Our results illuminate how loop extrusion contributes to actively modulate genome entanglement and viscoelasticity *in vivo*.

How chromosomes are packaged within the cell while remaining accessible to transcription, replication and segregation remains one of the most fascinating unsolved problems in physics and biology. Chromosome conformation capture (3C) and related techniques [1, 2] have revealed that chromosomes are folded into so-called territories, compartments and "Topologically Associated Domains" (TADs) [3–6]. Among the most important processes dictating chromosome folding in both interphase and mitosis is loop extrusion, performed by so-called Loop Extruding Factors (LEFs), such as cohesin, condensin and SMC5/6 [7–17]. Most of the current experimental techniques either study static snapshots of LEF-mediated chromosome conformation *in vivo* [16], or dynamic LEF-mediated looping process on tethered single DNA molecules *in vitro* [12]; and only very recently it was possible to track the behaviour of individual chromosome loci under the effect of loop extrusion [18]. Due to this, we still lack a quantitative understanding of how LEFs modulate chromosome dynamics and entanglements in the dense, crowded and entangled environment of the cell nucleus. To tackle this question we perform large-scale Molecular Dynamics simulations of entangled fluids of linear polymers under the action of LEFs. Specifically, we study how their number, processivity and turnover affect polymer conformation, dynamics and viscoelasticity.

First, we find that (exclusively intrachain) loop extrusion induces a transition from linear polymers to bottlebrush-like structures, characterised by large grafting density and side-chain length controlled by the number and processivity of the LEFs, in line with previous works in dilute conditions [9, 19, 20]. The formation of such structures reduces the entanglement between chains due to the entropic repulsion of side-chains [21, 22], thus leading to the fluidification of the system. Second, we discover that whilst as little as $\sim$ 2 - 100 LEFs per 30 kbp of chromatin is enough to induce a significant reduction in entanglement, a larger number of LEFs is not as effective due to a reduced entropic repulsion of side-chains and stiffening of the chain backbone. Strikingly, the extrusion enables an "active fluidification" process that can reduce the viscosity of long extruded polymers $\sim$ 1000-fold with respect to their non-extruded equivalent. Finally, we show that even LEFs with binding/unbinding kinetics can drive active fluidification in entangled fluids.

Our work is different from other simulations on LEF-mediated disentanglement of polymers [19, 23, 24] as we focus on the the bulk viscoelastic behaviour of dense polymer solutions, rather than segregation and compaction of isolated polymers. We argue that our results offer a novel perspective on loop extrusion and on how it impacts chromosome entanglement and genome fluidity. More specifically, our results suggest that by varying the number and processivity of LEFs, the cell may be able to finely regulate entanglements between chromosomes and, in turn, the nucleoplasm effective viscoelasticity, which could be tested in large-scale imaging and spectroscopy experiments [25–27].

Results. – We simulate entangled DNA as semi-flexible Kremer-Grest linear polymers [29] with $N = 250 - 1500$ beads, persistence length $l_p = 5\sigma$, and at volume fraction $\phi = 0.05$ (as physiologically relevant, see SI for other values of ϕ). We implement loop extrusion by loading, on average, n_{LEF} extruders per polymer, and moving the position of finitely extensible (FENE) bonds between beads along purely repulsive polymers [24]. Unlike previous extrusion models [9, 10, 19], the maximum extension of the FENE bonds is set such that it does not allow a third segment to pass through the LEF-mediated loop, thereby ensuring topological constraints are fully accounted for. Additionally, we account for the effect of polymer entropy on the loop extrusion speed by al-

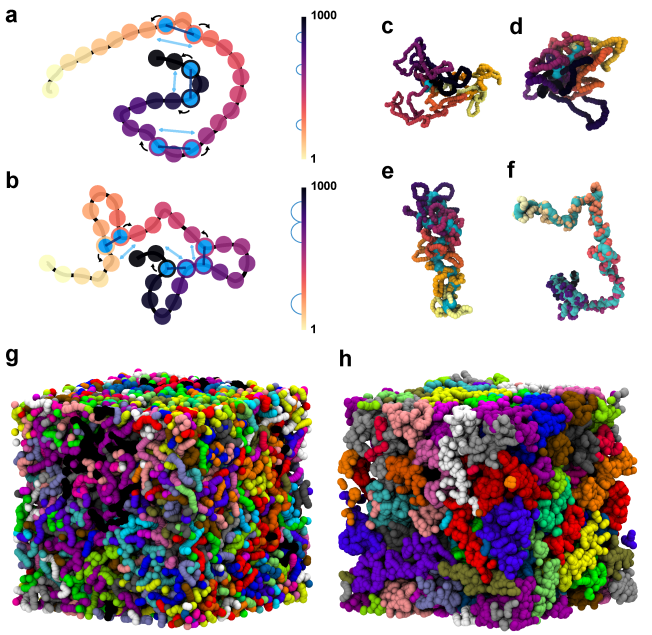

FIG. 1. **a-b** Sketches of our LEF algorithm on a coarse-grained polymer. **c-f** Snapshots of fully-extruded polymers with n_{LEF} = (c) 2, (d) 10 (e) 100 and (f) 200 and $N = 1000$. **g-h** Snapshots of (g) equilibrated non-extruded and (h) fully extruded chains with $n_{LEF} = 100$ and $N = 1000$. In panels a-f the color gradient represents bead index, while in panels g-h colors represent different polymers.

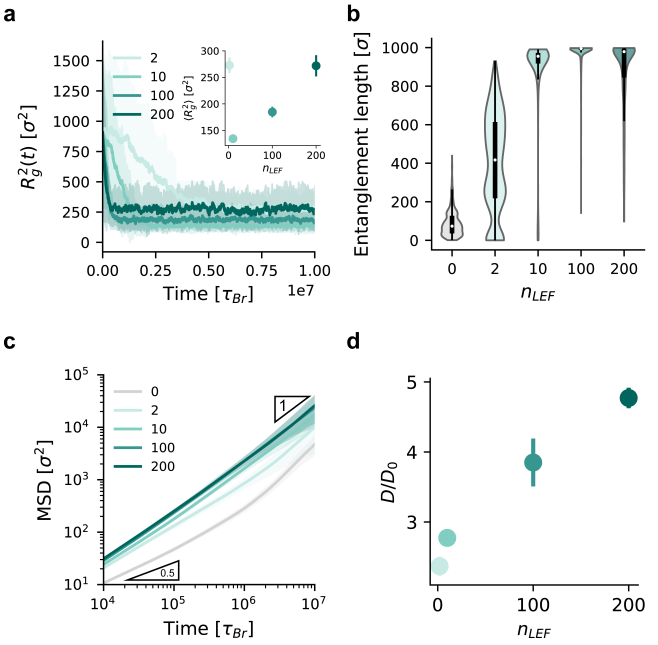

FIG. 2. **a** Average squared radius of gyration of $N = 1000$ beads long polymers during extrusion. The shaded area represents the standard deviation. The inset displays the equilibrium value against n_{LEF}. The equilibrium value of non-extruded chains is around $R_g^2 \simeq 10^3\sigma^2$. **b** Violin plot representing the distribution of entanglement lengths against n_{LEF} obtained through PPA [28]. **c** Ensemble and time average mean squared displacement (MSD) of the polymers' center of mass with its relative standard deviation (shaded area). **d** Diffusion coefficient of the polymers' CoM normalised to the non-extruded system as a function of n_{LEF}.

lowing the LEF bond to move only when the newly selected pair of beads are within a certain distance cut-off $r_{LEF} = 1.2\sigma$. In SI, we show that our LEF speed computed a posteriori is in line with experiments, i.e., around $v_{eff} \simeq 0.1$ kbp/s [12]. In contrast with recent works [30, 31], here we consider purely intrachain loop extrusion with no bridging interaction between LEFs (Fig. 1a-b). The simulations are then performed in an implicit solvent (Langevin) using the LAMMPS engine [32].

We first qualitatively observe that the extrusion induces a geometrical deformation of the polymers into bottlebrush-like structures [19, 20, 22] at fixed polymer length $N = 1000$ (Fig. 1c-f). Interestingly, this is accompanied by the onset of compartmentalisation and "territories", with the polymers becoming less intermingled [23] (see Fig. 1g-h, and movie M1). The radius of gyration R_g^2 (see SI) displays a sharp decrease during the extrusion process (Fig. 2a). At large time, the steady state value $\langle R_g^2 \rangle$ displays a non-monotonic behaviour, which we understand as direct consequence of the bottlebrush structure (e.g., see snapshots in Fig. 1c-f): larger number of LEFs effectively induce a larger grafting density and longer backbones, which contribute to an increase of R_g^2.

The non-monotonic compaction of the polymers is intriguing and it suggests that there may be a trade-off between compaction and effective rigidification of the backbone (see Fig. 1f). Additionally, denser, longer side loops typically yield stronger entropic repulsion [21]. To address the impact of this conformational transition on entanglements, we perform Primitive Path Analysis (PPA) [28, 33] (see SI for details). We find that non-extruded solutions have an average entanglement length $N_e = 89 \pm 46$. With as little as 2 LEFs per polymer, the mean entanglement length increases to $N_e = 404 \pm 200$ (Fig. 2b) and we observe a virtually fully disentangled state ($N_e = 975 \pm 4$) with 100 LEFs per polymer, i.e., $N/n_{LEF} = 10$. Further simulations with different values of N (250-1500) display total disentanglement for the same density of LEFs (see SI). Additionally, increasing the number of LEFs leads to a mild re-entanglement, due to the non-monotonic compaction we uncovered previously and to the fact that side-loops are shorter.

Having quantified the dramatic change in the static properties of the solution, we expect to observe a similar large impact of extrusion on the dynamics. In Fig. 2c, we show that the mean squared displacement (MSD) of the polymers center of mass (CoM) displays a significant speed up compared with the non-extruded case. More specifically, the diffusion coefficient of the polymers CoM,

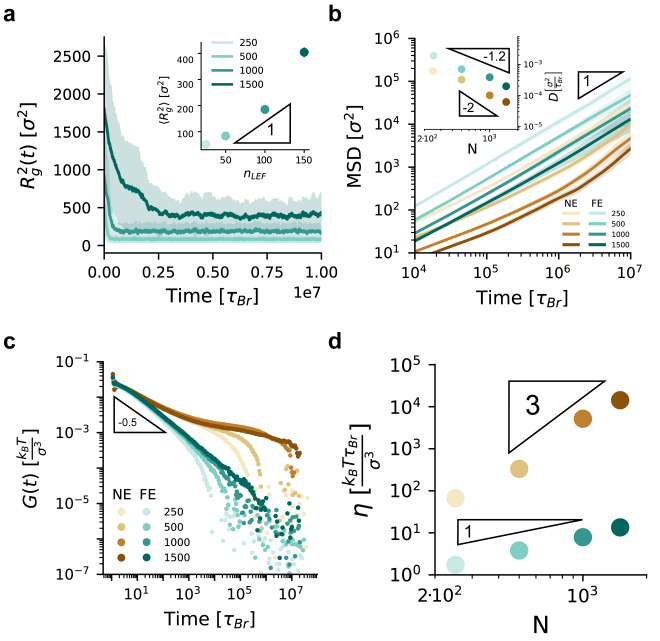

FIG. 3. **a** Average squared radius of gyration of polymers during extrusion for different N. The inset displays the equilibrium value against n_{LEF}. **b** Average mean squared displacement (MSD) of the polymers' center of mass for non-extruded (NE, brown) and fully extruded (FE, green) systems. The inset displays the diffusion coefficient of the polymers' centers of mass against the polymer length. **c** Stress-relaxation function of non-extruded (NE, brown) and fully-extruded (FE, green) solutions. **d** Viscosity of extruded and non-extruded systems obtained by integration of the stress-relaxation function.

computed as $D = \lim_{t\to\infty} \mathrm{MSD}/6t$ in the system with $N/n_{LEF} = 5$ (or $n_{LEF} = 200$) is roughly 5 times larger than the control. Intriguingly, we observe an increase in mobility of the polymers even though the system is nearly fully disentangled at smaller $n_{LEF} = 10$. We argue that this may be due to the further rigidification of the polymers.

Our results thus suggest that purely intrachain loop extrusion leads to an effective "active fluidification" due to the transition from linear to bottlebrush-like structures. We argue that this fluidification ought to be even more dramatic in more entangled solutions (e.g. denser or made of longer chains). Ultimately, we would like to understand how LEF-mediated fluidication affects the entanglement and viscoelasticity of genome-size DNA. To this end, we perform simulations with shorter ($N = 250$, $N = 500$) and longer ($N = 1500$) chains at fixed volume fraction ($\phi = 0.05$) and fixed LEF densities ($N/n_{LEF} = 10$). First, we discover that loop extrusion compacts all polymer lengths down to similar sizes and that the steady state $\langle R_g^2 \rangle$ scales roughly linearly with n_{LEF}, which is consistent with the expected scaling [22] $R_g^2 \sim L_{bb} L_{sl}^{1/2}$, where L_{bb} is the length of the backbone (determined by the number of extruders) and L_{sl} the length of side loops (determined by N/n_{LEF}).

As before, we compare the dynamics of the CoM MSD and find that in all extruded solutions there is a clear loss of the early-time subdiffusive regime (Fig. 3b). For non-extruded configurations, the diffusion coefficient of the CoM scales as $D \sim N^{-1.6}$, close to $D \sim N^{-2}$ expected for reptative dynamics [34]. On the other hand, for extruded solutions we find $D \sim N^{-1.2}$.

To quantify the change in viscoelasticity due to the extrusion, we use the Green-Kubo relation and compute the autocorrelation of the off-diagonal components of the stress-tensor $G(t)$ [35] (see SI). The familiar entanglement plateau observed for linear polymers [29] is completely lost in all extruded solutions, which instead follow a decay $G(t) \sim t^{-1/2}$ (Fig. 3c). We interpret this as a strong signature that most of the entanglements are lost, even for our longest polymers $N = 1500$, which have $N/N_e \simeq 17$ at equilibrium. Perhaps more remarkably, the viscosity $\eta = \int_0^\infty G(t)dt$, which displays the usual $\eta \sim N^3$ scaling for the case of linear polymers, scales only linearly ($\eta \sim N$) in the fully extruded case (Fig. 3d). These findings strongly suggest that the active fluidification mechanism is more dramatic in solutions of longer polymers as, $\eta_{LEF}/\eta_0 \sim N^{-2}$. For example, for $N = 1500$, the viscosity of the extruded system is about 1000 times smaller than the non-extruded one. Furthermore, we find even stronger fluidification in denser systems (see SI). Extrapolating these results to genomic-size DNA, we expect the difference between the dynamics of chromosomes in presence/absence of (purely intrachain and non-bridging) LEFs will be several orders of magnitude. This implies that the large-scale rearrangement and dynamics of interphase and mitotic chromosomes are expected to be sensitive to the presence of active loop extrusion and may be tested in experiments via, e.g., displacement correlation spectroscopy or other imaging methods [18, 25, 36–38].

Dynamic Loop Extrusion. – Having quantified the fluidification achieved in a fully-extruded steady state, we now turn our attention to the behaviour of our system under a non-equilibrium, dynamic loop extrusion process in which LEFs load/unload dynamically at rates κ_{on} and κ_{off} for $N = 1000$. The total number of LEFs in the simulation is fixed, but the number bound at any one time fluctuates around the mean fraction $f_{bound} = \kappa_{on}/(\kappa_{on} + \kappa_{off})$. In the following, we focus on the so-called "partially extruded" case, in which the total extruded length is smaller than N, i.e. the LEFs kinetically unbind from the polymer before they can fully extrude the average distance between them (see Fig. 4a). We highlight that the regime of partial extrusion is the one that appears to be most relevant *in vivo* [18], and can be characterised by the ratio between the average processivity and the average spacing between LEFs, i.e. $\langle p \rangle / \langle d \rangle = \langle v_{LEF} \rangle / \kappa_{off} \times N/n_{LEF}$ (see Fig. 4b). In partially extruded solutions $\langle p \rangle / \langle d \rangle < 1$.

First, we find that the radius of gyration of the poly-

mers depends on $\langle p \rangle / \langle d \rangle$: small values yield non-extruded polymers, while larger values yield a compaction similar to the fully extruded case (where $\langle p \rangle / \langle d \rangle \to \infty$ as $k_{off} = 0$). Interestingly, we also observe stable, intermediate compacted states in between a fully extruded and non-extruded state where the polymer is kept out-of-equilibrium by the kinetic binding/unbinding of LEFs (Fig. 4d).

To make a comparison with experiments, we compute the 2-point MSD [18, 36], i.e., the autocorrelation of the distance vector $\boldsymbol{d}$ between two given polymer segments separated by the curvilinear distance l or $2\text{pMSD}(t, l) = \langle [\boldsymbol{d}(t_0 + t, s + l) - \boldsymbol{d}(t_0, s)]^2 \rangle_{t_0, s}$. In line with recent experiments [18, 36, 37] and Rouse theory, we observe a short-time scaling $2\text{pMSD}(t) \sim t^{1/2}$ that is surprisingly unaffected by loop the extrusion (Fig. 4e). A quantitative different behaviour of the $2\text{pMSD}(t)$ is seen only at large times due to the different polymer compaction, in agreement with experiments implementing rapid cohesin knockouts [18]. At intermediate timescales, both the non-extruded and partially extruded cases display $2\text{pMSD}(t) \sim t^{1/3}$, which is consistent with the one observed in experiments with embryo cells [36].

Finally, we also compute the stress relaxation function $G(t)$ for this out-of-equilibrium partially extruded scenario and once again we observe a clear lack of entanglement plateau in the presence of LEFs. In turn, this translates in a significantly smaller effective viscosity of the partially extruded solution, which depends on the dimensionless ratio $\langle p \rangle / \langle d \rangle$. For partially extruded solutions with $\langle p \rangle / \langle d \rangle \simeq 1$ the viscosity is 100-fold smaller than the control case, and we expect to display the same scaling with the polymer length seen in Fig. 3.

Conclusions. – Motivated by the lack of understanding of how loop extrusion affects polymer entanglement and dynamics in dense solutions, we performed large-scale molecular dynamics simulations of entangled polymers under the action of loop extruding factors. The first main discovery of our work is that loop extrusion, when is a fully intrachain process, dramatically decreases the entanglement between chains, and fully extruded chains display no sign of entanglement and, in fact, display an emergent territorial organisation (Figs. 1-2). We then discovered that the mobility of the polymers is strongly sped up by the extrusion process, in turn yielding an effective active fluidification of the solutions and leading to viscosity reduction up to 1000-fold (Fig. 3). Finally, we considered the case of partial extrusion using a kinetic binding model and showed that even in the partially extruded situation, with kinetic binding/unbinding of LEFs, the viscosity of polymer solutions is greatly reduced via the active extrusion process (Fig. 4).

Our findings suggest that loop extrusion may have a marked effect on the large-scale organisation and viscoelasticity of the nucleoplasm, through the change in conformation and dynamics of chromosomes. We note

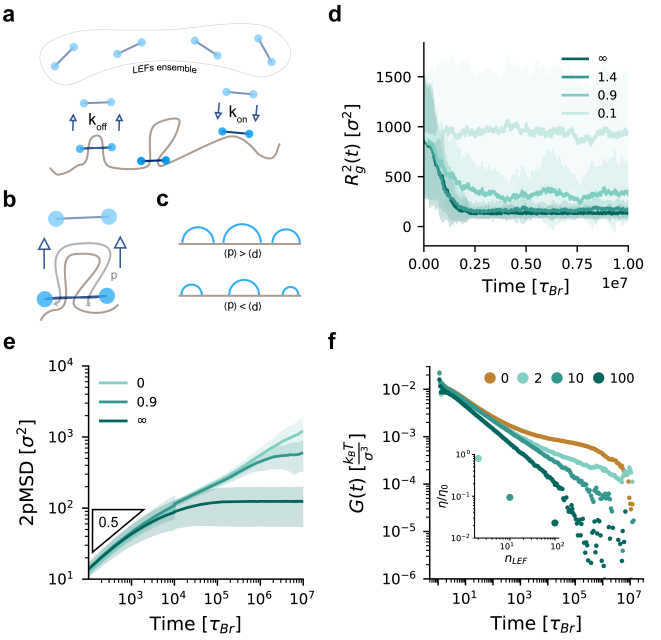

FIG. 4. **a** Sketch of our kinetic extrusion model. LEFs perform extrusion until they are removed at rate k_{off}, whilst unbound LEFs can load and start extruding at rate k_{on}. **b** Sketch of how processivity (p) is computed, i.e., by measuring the length of polymer covered by LEF before unbinding. **c** Sketch of extruded systems for different processivity: $\langle p \rangle > \langle d \rangle$ yields fully extruded polymers, whilst $\langle p \rangle < \langle d \rangle$ yields partially extruded polymers. **d** Average squared radius of gyration during extrusion for different values of $\langle p \rangle / \langle d \rangle$. **e** 2-point MSD computed at contour distance of $l = 600$ beads for systems with different values of $\langle p \rangle / \langle d \rangle$. **f** Stress-relaxation function for non-extruded (brown) and partially extruded (green) systems with $\langle p \rangle / \langle d \rangle \simeq 1$ and different values of n_{LEF}. The inset displays the relative viscosity normalised to the viscosity of the non-extruded system and shows up to $\simeq 100$-fold reduction in these conditions.

that our results are strongly dependent on the fact that we assumed loop extrusion to be solely intrachain. Interchain loop extrusion [30] and bridging [31] may drastically influence our results, eventually decreasing the mobility of the polymers and thus increasing the viscoelasticity of the solution. We will test this hypothesis in the near future.

Acknowledgements. – DM acknowledges the Royal Society and the European Research Council (grant agreement No 947918, TAP) for funding. The authors also acknowledge the contribution of the COST Action Eutopia, CA17139. For the purpose of open access, the author has applied a Creative Commons Attribution (CC BY) licence to any Author Accepted Manuscript version arising from this submission.

[1] E. Lieberman-Aiden, N. L. van Berkum, L. Williams, M. Imakaev, T. Ragoczy, A. Telling, I. Amit, B. R. Lajoie, P. J. Sabo, M. O. Dorschner, R. Sandstrom, B. Bernstein, M. a. Bender, M. Groudine, A. Gnirke, J. Stamatoyannopoulos, L. a. Mirny, E. S. Lander, and J. Dekker, Science **326**, 289 (2009).

[2] R. A. Beagrie, A. Scialdone, M. Schueler, D. C. A. Kraemer, M. Chotalia, S. Q. Xie, M. Barbieri, I. de Santiago, L.-M. Lavitas, M. R. Branco, J. Fraser, J. Dostie, L. Game, N. Dillon, P. A. W. Edwards, M. Nicodemi, and A. Pombo, Nature **543**, 519 (2017).

[3] T. Cremer and C. Cremer, Nat. Rev. Genet. **2**, 292 (2001).

[4] C. Brackley, M. Pereira, J. Johnson, D. Michieletto, and D. Marenduzzo, Modeling the 3D Conformation of Genomes , 97 (2019).

[5] J. Dekker, M. A. Marti-Renom, and L. A. Mirny, Nature Reviews Genetics **14**, 390 (2013).

[6] J. Nuebler, G. Fudenberg, M. Imakaev, N. Abdennur, and L. A. Mirny, Proceedings of the National Academy of Sciences of the United States of America **115**, E6697 (2018).

[7] K. Nasmyth, Nature Cell Biology **13**, 1170 (2011).

[8] E. Alipour and J. F. Marko, Nucleic Acids Res. **40**, 11202 (2012).

[9] G. Fudenberg, M. Imakaev, C. Lu, A. Goloborodko, N. Abdennur, and L. A. Mirny, Cell Reports **15**, 2038 (2016).

[10] A. L. Sanborn, S. S. P. Rao, S.-C. Huang, N. C. Durand, M. H. Huntley, A. I. Jewett, I. D. Bochkov, D. Chinnappan, A. Cutkosky, J. Li, K. P. Geeting, A. Gnirke, A. Melnikov, D. McKenna, E. K. Stamenova, E. S. Lander, and E. L. Aiden, Proc. Natl. Acad. Sci. USA **112**, 201518552 (2015).

[11] I. F. Davidson, B. Bauer, D. Goetz, W. Tang, G. Wutz, and J.-M. Peters, Science **366**, 1338 (2019).

[12] M. Ganji, I. A. Shaltiel, S. Bisht, E. Kim, A. Kalichava, C. H. Haering, and C. Dekker, Science **360**, 102 (2018).

[13] B. Pradhan, T. Kanno, M. Umeda Igarashi, M. S. Loke, M. D. Baaske, J. S. K. Wong, K. Jeppsson, C. Björkegren, and E. Kim, Nature **616**, 843 (2023).

[14] A. S. Câmara, V. Schubert, M. Mascher, and A. Houben, Nucleic Acids Research **49**, 9053 (2021).

[15] L. Vian, A. Pękowska, S. S. Rao, K. R. Kieffer-Kwon, S. Jung, L. Baranello, S. C. Huang, L. El Khattabi, M. Dose, N. Pruett, A. L. Sanborn, A. Canela, Y. Maman, A. Oksanen, W. Resch, X. Li, B. Lee, A. L. Kovalchuk, Z. Tang, S. Nelson, M. Di Pierro, R. R. Cheng, I. Machol, B. G. St Hilaire, N. C. Durand, M. S. Shamim, E. K. Stamenova, J. N. Onuchic, Y. Ruan, A. Nussenzweig, D. Levens, E. L. Aiden, and R. Casellas, Cell **173**, 1165 (2018).

[16] J. H. Gibcus, K. Samejima, A. Goloborodko, I. Samejima, N. Naumova, J. Nuebler, M. T. Kanemaki, L. Xie, J. R. Paulson, W. C. Earnshaw, L. A. Mirny, and J. Dekker, Science **359**, eaao6135 (2018).

[17] M. Conte, E. Irani, A. M. Chiariello, A. Abraham, S. Bianco, A. Esposito, and M. Nicodemi, Nature Communications **13** (2022).

[18] M. Gabriele, H. B. Brandão, S. Grosse-Holz, A. Jha, G. M. Dailey, C. Cattoglio, T.-H. S. Hsieh, L. Mirny, C. Zechner, and A. S. Hansen, (2022).

[19] A. Goloborodko, J. F. Marko, and L. A. Mirny, Biophysical Journal **110**, 2162 (2016).

[20] E. J. Banigan and L. A. Mirny, Physical Review X **9**, 031007 (2019).

[21] J. F. Marko and E. D. Siggia, Molecular Biology of the Cell **8**, 2217 (1997).

[22] J. Paturej, S. S. Sheiko, S. Panyukov, and M. Rubinstein, Science Advances **2**, e1601478 (2016).

[23] D. Racko, F. Benedetti, D. Goundaroulis, and A. Stasiak, Polymers **10**, 1 (2018).

[24] E. Orlandini, D. Marenduzzo, and D. Michieletto, in *Proceedings of the National Academy of Science USA*, Vol. 116 (2019) p. 8149.

[25] A. Zidovska, D. A. Weitz, and T. J. Mitchison, Proceedings of the National Academy of Sciences of the United States of America **110**, 15555 (2013).

[26] D. Saintillan, M. J. Shelley, and A. Zidovska, Proceedings of the National Academy of Sciences of the United States of America **115**, 11442 (2018).

[27] C. M. Caragine, S. C. Haley, and A. Zidovska, Physical Review Letters **121**, 148101 (2018).

[28] R. Everaers, S. K. Sukumaran, G. S. Grest, C. Svaneborg, A. Sivasubramanian, and K. Kremer, Science **303**, 823 (2004).

[29] K. Kremer and G. S. Grest, The Journal of Chemical Physics **92**, 5057 (1990).

[30] A. Bonato and D. Michieletto, Biophysical Journal **120**, 5544 (2021).

[31] J.-K. Ryu, C. Bouchoux, H. W. Liu, E. Kim, M. Minamino, R. de Groot, A. J. Katan, A. Bonato, D. Marenduzzo, D. Michieletto, F. Uhlmann, and C. Dekker, Science Advances **7**, eabe5905 (2021).

[32] S. Plimpton, J. Comp. Phys. **117**, 1 (1995).

[33] N. Uchida, G. S. Grest, and R. Everaers, The Journal of Chemical Physics **128**, 044902 (2008).

[34] M. Doi and S. Edwards, *The theory of polymer dynamics* (Oxford University Press, 1988).

[35] J. Ramírez, S. K. Sukumaran, B. Vorselaars, and A. E. Likhtman, J . Chem. Phys. **133**, 154103 (2010).

[36] A. K. Yesbolatova, R. Arai, T. Sakaue, and A. Kimura, Physical Review Letters **128**, 178101 (2022).

[37] D. B. Brückner, H. Chen, L. Barinov, B. Zoller, and T. Gregor, Science **380**, 1357 (2023).

[38] H. A. Shaban, R. Barth, and K. Bystricky, Nucleic Acids Research **46** (2018), 10.1093/nar/gky269.

Active Fluidification of Entangled Polymers by Loop Extrusion: Supplementary Information

Filippo Conforto,[1] Yair Augusto Gutierrez Fosado,[1] and Davide Michieletto[1,2]

[1] *School of Physics and Astronomy, University of Edinburgh, Peter Guthrie Tait Road, Edinburgh, EH9 3FD, UK*

[2] *MRC Human Genetics Unit, Institute of Genetics and Cancer, University of Edinburgh, Edinburgh EH4 2XU, UK*

SIMULATION DETAILS

We model polymers as semi-flexible coarse-grained bead-spring polymers with $N = 250$, $N = 500$, $N = 1000$ and $N = 1500$ beads of size σ. The beads interact with each other via a truncated and shifted Lennard-Jones potential,

$$U_{\rm LJ}(r) = \begin{cases} 4\epsilon\left[\left(\frac{\sigma}{r}\right)^{12} - \left(\frac{\sigma}{r}\right)^{6} + \frac{1}{4}\right] & r \leq r_c \\ 0 & r > r_c \end{cases}, \quad (1)$$

where r denotes the separation between the beads and the cut-off $r_c = 2^{1/6}\sigma$ is chosen so that only the repulsive part of the potential is used. Nearest-neighbour monomers along the contour of the chains are connected by finitely extensible nonlinear elastic (FENE) springs as,

$$U_{\rm FENE+LJ}(r) = \begin{cases} -0.5kR_0^2 \ln\left(1 - (\frac{r}{R_0})^2\right) + U_{\rm LJ} & r \leq R_0 \\ \infty & r > R_0 \end{cases}, \quad (2)$$

where $k = 30\epsilon/\sigma^2$ is the spring constant and $R_0 = 1.5\sigma$ is the maximum extension of the elastic FENE bond. This choice of potentials and parameters is essential to preclude thermally-driven strand crossings and therefore ensures that the global topology is preserved at all times [1]. Finally, we add bending rigidity via a Kratky-Porod potential, $U_{\rm bend}(\theta) = k_\theta\left(1 - \cos\theta\right)$, where θ is the angle formed between consecutive bonds and $k_\theta = 5k_BT$ is the bending constant, thus yielding a persistence length $l_p = 5\sigma$, corresponding to 50 nm in our coarse grained model. Each bead's motion is then evolved via the Langevin equation

$$m\frac{dv_i}{dt} = -\gamma v_i - \nabla U + \sqrt{2k_BT\gamma}\eta_i \quad (3)$$

along each Cartesian component. Here, γ is the friction coefficient, m the mass of the bead, U the sum of the potentials acting on bead i and $\sqrt{2k_BT\gamma}\eta_i$ a noise term that obeys the fluctuation-dissipation theorem, thus respecting the formula

$$\langle \eta_i^\alpha(t)\eta_j^\beta(s)\rangle = \delta(t-s)\delta_{ij}\delta_{\alpha\beta}$$

along each Cartesian component (Greek letters). The numerical evolution of the Langevin equation is done with a velocity-Verlet scheme with $dt = 0.01\tau_{LJ}$ with $\tau_{LJ} = \tau_{Br} = \sigma\sqrt{m/\epsilon}$ in LAMMPS [2]. Four different systems were considered during this work: 250, 500, 1000, 1500 beads-long polymers with monomer density of about 10% (equivalent to a volume fraction $\phi = 0.05$). The boxes have linear dimension of 51σ, 64σ, 80.6σ and 92σ, respectively. Each simulation has 50 polymers.

MODELLING LOOP EXTRUSION

We based our loop extrusion model on previous work [3–5], with the main difference that our loop extruding factors (LEFs) can make forward steps only if the distance between the new pair of selected beads is smaller than a small cutoff $< 1.2\sigma$ and we use FENE bonds rather than harmonic bonds. This makes sure that it is not possible for the LEF to pass through a third polymer strand and thus our model fully accounts for realistic topological constraints exerted by loop extruding proteins on DNA or chromatin. This model was tested in Ref. [5], where we confirmed topology conservation by performing loop extrusion on knotted polymers. Below, we describe in detail our loop extrusion model.

At the beginning of the simulation we deposit a set of LEFs by choosing random triplets of beads along the chains. This provides each polymer with a total number of bounded LEFs on average equal to n_{LEF}. However, to avoid the presence of unextruded polymers we deploy at least one LEF on every polymer. A LEF is modelled by creating a bond between two beads along a chain (separated by one bead). Loop extrusion is then achieved by moving the bond to the adjacent beads on both sides, as shown in figure 1a of the main text. Specifically, we attempt extrusion steps with a fixed frequency f_{att}, chosen at the beginning of the simulation, and then we define a success probability f_{prob} for the extrusion step. Then, the distance between the new LEFs "heads" is computed and the step is accepted only if its value is smaller than a fixed cut-off $r < 1.2\sigma$. Effectively each LEF attempts a step with frequency $f_{eff} = f_{att}f_{prob} = 1 \times 10^{-3}\,\tau_{\rm Br}{}^{-1}$. We note that its speed is also affected by the local geometry of the polymer. For instance, regions of high entropy or tension will slow down the LEF motion by keeping the polymer beads away from each other. Thus, the polymer entropy has an explicit effect on the motion of the LEF,

which is otherwise absent in other models in the literature.

To prevent numerical instabilities, we employ a harmonic bond for the first step of the extrusion, with potential

$$U_{\text{harm}}(r) = A(r - R_0)\,, \tag{4}$$

where $A = 100$ and $R_0 = 1.1\sigma$. After the first step, such bond is replaced by a FENE bond with $k = 10\epsilon/\sigma^2$ and $R_0 = 1.7\sigma$ (see Eq. 2). We choose a larger maximum extension for the LEF FENE bond and a softer spring constant to avoid bond breaking caused by sudden movement of the bonds during extrusion.

If during the extrusion process two LEFs meet along the chain, extrusion proceeds only on the free side, as displayed in figure 1b. Consequently extrusion runs for each LEF until one of its ends neighbours another LEF's head or reaches the polymer ends.

To implement this in LAMMPS [6] we developed a custom fix module publicly available at `https://git.ecdf.ed.ac.uk/s2469797/smc-lammps.git`, and used the version v30_06_23 for this work.

MEAN SQUARED DISPLACEMENT AND RADIUS OF GYRATION

The ensemble and time averaged mean squared displacement (MSD) at time τ measures the average deviation of the position of a particle with respect to the initial position over a time τ. It is computed as

$$\text{MSD}(\tau) = \frac{1}{M}\frac{1}{T-\tau}\sum_{i=1}^{M}\sum_{t=0}^{T-\tau}\left[\boldsymbol{r}^i_{com}(t+\tau) - \boldsymbol{r}^i_{com}(t)\right]^2\,,$$

where $\boldsymbol{r}^i_{com}$ are the polymer COM coordinates, and M is the number of polymers in the box. For entangled linear polymers we expect the MSD of the polymer's center of mass (COM) $\text{MSD}(\tau) \sim \tau^{\frac{1}{2}}$ for short timescales and $\text{MSD}(\tau) \sim \tau$ on long timescales [7]. The squared radius of gyration of a polymer is computed as

$$R_g^2 = \frac{1}{N}\sum_{k=1}^{N}\left[\boldsymbol{r}_k - \boldsymbol{r}_{com}\right]^2$$

where $\boldsymbol{r}_k$ defines the coordinates of the polymer beads, and N is the polymer length.

PRIMITIVE PATH ANALYSIS

Primitive path analysis is a technique used to compute the entanglement length (distance between two entanglements) and thus the degree of entanglement of a solution [8]. We apply this method by choosing 10 restart configurations from each trajectory, sampled at times separated by $1 \times 10^5 \tau_{\text{Br}}$ to sample uncorrelated conformations. We then fixed the position of the polymer ends in space and set the equilibrium distance of the polymer bonds to 0 (remove the repulsion via LJ, but keep the FENE potential). At the same time, we remove pair repulsion between beads belonging to the same polymer and quench the system to temperature 0. We perform 5 of these simulations for each sampled configuration with different integration seeds. The systems thus obtained achieve the primitive path with notable kinks at entanglement points (see Fig, S1), from which the entanglement length can be computed as

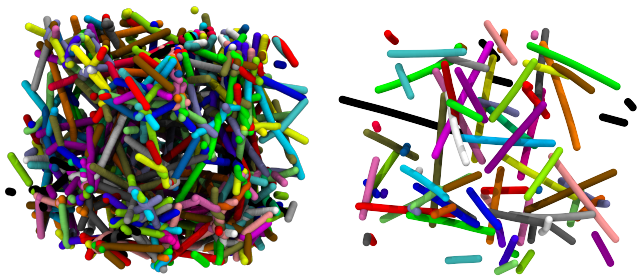

FIG. S1. Snapshot of simulated PPA for a (left) non extruded and (right) fully extruded solutions.

$$L_e = \frac{D^2_{e2e}}{N \cdot \overline{D_{bond}}^2}$$

where D_{e2e} represents the end to end distance of the polymer, and $\overline{D_{bond}}$ the average bond length in the polymer.

The assumption for this formula is that the coils are Gaussian so we also computed the tangent-tangent correlation along the primitive paths as

$$\alpha_n = \langle t_{i+n} \cdot t_i \rangle = \frac{1}{N-n}\sum_{i=1}^{N-n} t_{i+n} \cdot t_i \tag{5}$$

where t_i is the tangent of the i-th segment of the curve and α_n represents the average correlation between tangents separated by n segments. This value is expected to decay as

$$\alpha(n) = e^{-\frac{n}{\lambda}} \tag{6}$$

where λ is a correlation length, and can be then fitted numerically. Disentangled polymers appears to be straight after PPA (see Fig. S1), and the correlation length can assume arbitrarily large values, we thus cap λ to double the polymer length for consistency. We finally estimate the entanglement length as $\lambda/2$ (see Fig. S2). The result from this analysis yields the same behaviour as the one obtained using the original PPA equation. See Figs. 2b of the main text and Fig. S2.

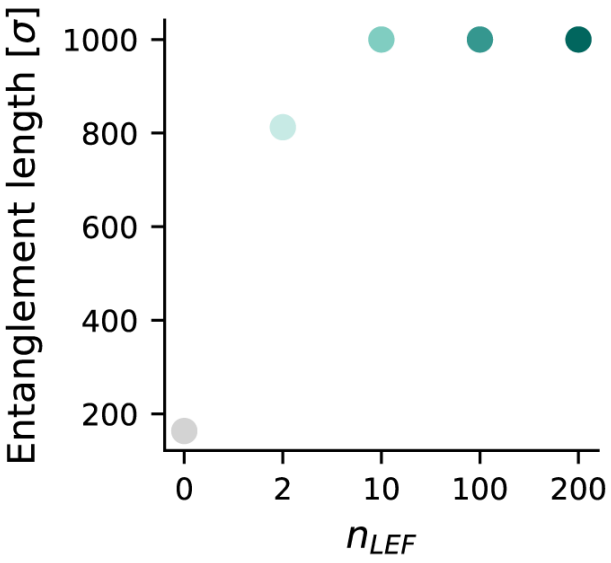

FIG. S2. Average entanglement length computed as $\frac{\lambda}{2}$, where λ is the fitted exponent of the tangent-tangent correlation function (eq. (6)).

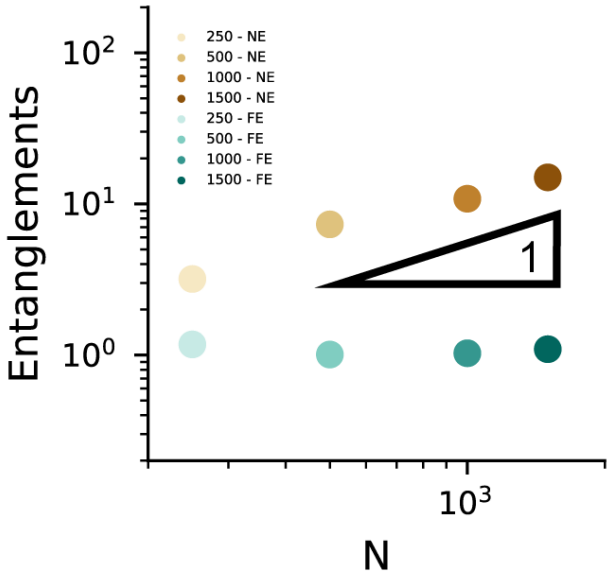

FIG. S3. Number of entanglements for fully extruded (FE) and non-extruded (NE) configurations with different polymer lengths (from $N = 250$ to $N = 1500$ beads), with same LEF density ($N/n_{LEF} = 10$).

GREEN-KUBO RELATIONS

The stress-relaxation modulus $G(t)$ is calculated as

$$G(t) = \frac{V}{3k_bT}\sum_{\alpha\neq\beta}\bar{P}_{\alpha\beta}(0)\bar{P}_{\alpha\beta}(t)\,,$$

where ($\bar{P}_{\alpha\beta} = \bar{P}_{xy}$ and $\bar{P}_{xz}$ and $\bar{P}_{yz}$) represents the off-diagonal components of the stress tensor. Specifically we get those components as

$$\bar{P}_{\alpha\beta}(t) = \frac{1}{t_{avg}}\sum_{\Delta t=-\frac{t_{avg}}{2}+1}^{t_{avg}} P_{\alpha\beta}(t+\Delta t)\,,$$

$$P_{\alpha\beta}(t) = \frac{1}{V}\left(\sum_{k=1}^{NM} m_k v_k^\alpha v_k^\beta + \frac{1}{2}\sum_{k=1}^{NM}\sum_{l=1}^{NM} F_{kl}^\alpha r_{kl}^\beta\right),$$

where N is the number of beads per polymer, M the number of polymers, V the box volume, m_k the mass of the k-th bead, v_k the speed of the k-th bead, F_{kl} the force between the k-th and the l-th bead and r_{kl} their distance. $P_{\alpha\beta}$ is then averaged over a time t_{avg} [9]. The autocorrelation was computed using the multiple-tau correlator method described in reference [10] and implemented in LAMMPS with the fix ave/correlate/long command. This method makes sure that the systematic error of the multiple-tau correlator to be always below the level of the statistical error of a typical simulation (see LAMMPS documentation). The viscosity η of the system is then obtained by integrating $G(t)$ as,

$$\eta = \int_0^\infty G(t)dt\,.$$

To account for the noisy values appearing on large timesteps we fit $G(t)$ with a stretched exponential at large times. Specifically, we define $G(t) = ae^{\left(\frac{t}{\tau}\right)^b}$, and we fit a, τ, b, starting at an arbitrary time t_e. The viscosity is then obtained by numerical integration up to t_e, summed up to the stretched exponential contribution, obtained by computing $\int_{t_e}^\infty ae^{\left(\frac{t}{\tau}\right)^b} = \frac{a\tau}{b}\Gamma\left(\frac{1}{b}, (\frac{t_e}{\tau})^b\right)$, where $\Gamma(a,z)$ is the upper generalised gamma function. The sum between these two terms returns the viscosity estimate.

LOOP EXTRUSION IS A LENGTH-INDEPENDENT DISENTANGLEMENT MECHANISM

It is interesting to notice that whilst the number of entanglements per polymer increases linearly with polymer length in entangled conditions, this quantity displays a fixed and constant value of 1 for fully extruded polymers, irrespectively of their length. This is shown in Fig. S3, where we display the results of PPA for systems with 1 LEF every 10 beads, and for a range of polymer lengths.

ACTIVE FLUIDIFICATION IS DENSITY DEPENDENT

To understand how the system density affects the extrusion-mediated fluidification we simulate a system of $M = 50$ polymers with $N = 1000$ and volume fraction

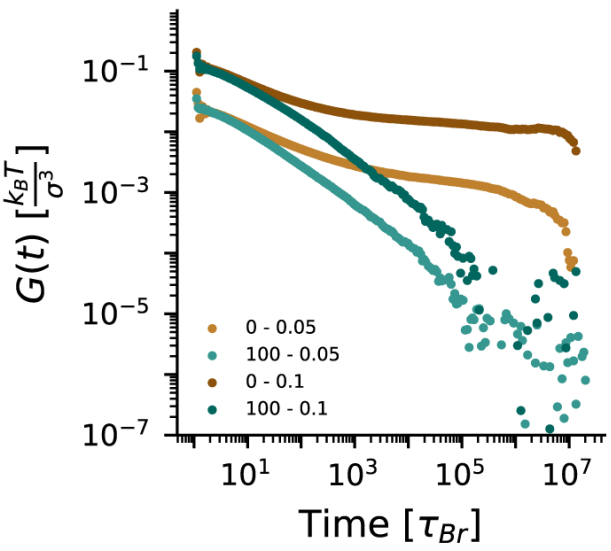

FIG. S4. Stress-correlation function of two $N = 1000$ beads-long polymer systems with different volume fractions (0.05 and 0.1). Green circles represent fully extruded systems with $n_{LEF} = 100$ (or $N/n_{LEF} = 10$), while brown circles correspond to non-extruded systems.

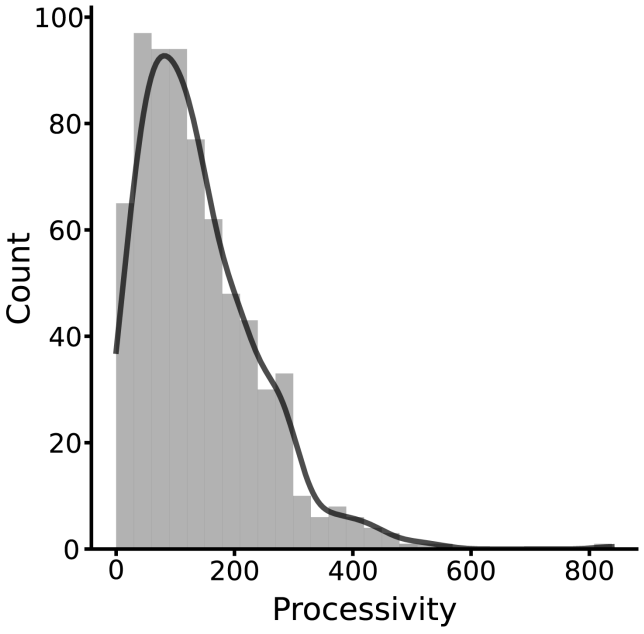

FIG. S5. Distribution of the processivity p during transient extrusion with an average of 10 LEFs per polymer. We measure this as the length covered by single LEFs before being removed from the polymer.

$\phi = 0.1$ (in the main text we consider $\phi = 0.05$). The stress-correlation function $G(t)$ shown in Fig. S4 displays a qualitatively similar fluidification properties. Indeed, the entanglement plateau is lost after extrusion. The viscosity computed from $G(t)$ computed for the denser system is ≈2000-fold lower than that for the non-extruded case at same density $\phi = 0.1$. On the other hand, for $\phi = 0.05$ we observe a fluidification ≈1000-fold. This suggests that the active fluidification will be more dramatic at larger polymer densities and lengths.

PROCESSIVITY

We can define the LEF processivity as $p = v_{LEF}/k_{off}$, but in practice the LEFs speed depends on the entropy, geometry and tension applied to the polymer. In the case of dynamic binding/unbinding, we computed the single LEF processivity as the length covered by single LEFs before being removed from the polymer. We can thus define the processivity as the average of this distribution, which is found to be Poissonian, in agreement with our stochastic LEF unbinding (see figure S5).

In figure S6 we display the squared radius of gyration against the average processivity divided by the average distance between LEFs on a polymer. When the normalised processivity is $\langle p\rangle/\langle d\rangle > 1$, the radius of gyration is similar to the one for the fully extruded case. When the normalised processivity is small ($\langle p\rangle/\langle d\rangle < 1$) we observe a radius of gyration close to the unextruded case. For intermediate values we find a novel and non-equilibrium steady state with radius of gyration roughly independent on the total number of LEFs in the system.

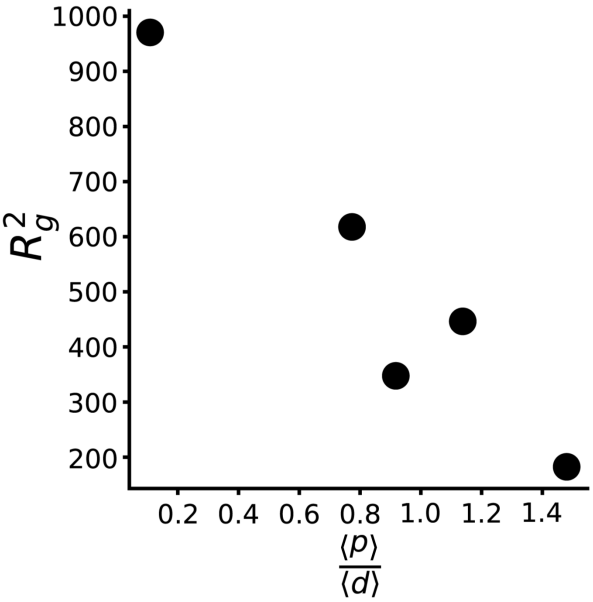

FIG. S6. Squared radius of gyration depends on the processivity and display a roughly linear decrease with against normalised processivity $\langle p\rangle/\langle d\rangle$.

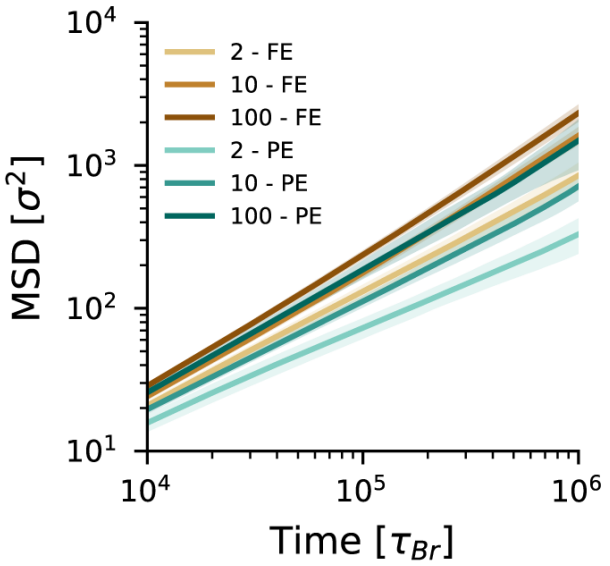

FIG. S7. Average Mean Squared Displacement(MSD) for the center of mass of fully extruded (FE) and partially extruded polymers (PE) with normalised processivity close to 1 and different n_{LEF} (2 - 100).

COMPARISON WITH EXPERIMENTAL DATA

Evidence show that SMCs extrusion speed is on the order of $1\,\mathrm{kbp\,s^{-1}}$ [11]. In our simulations, the maximum speed is obtained by assuming that all the moves are accepted, thus $v_{max} = 2\sigma \circ f_{eff} = 2 \cdot 10^{-3}\sigma\tau_{Br}^{-1}$ for $f_{eff} = 10^{-3}\tau_{Br}^{-1}$. Assuming each bead coarse grains ~ 30bp (or 10 nm), we have $v_{max} \simeq 26\,\mathrm{kbp\,s^{-1}}$. However, this maximum speed is rarely reached during simulations because of our stepping algorithm. We can get an estimate of the effective extrusion speed by multiplying the average processivity (from the distribution of single LEFs processivities) by the unbinding rate k_{off} (a fixed value imposed at the beginning of the simulation). For values of $\langle p\rangle/\langle d\rangle \sim 1$ this speed is found to be in the order of $10^{-5}\sigma\tau_{Br}^{-1}$ which converts to an effective speed around $v_{eff} \simeq 0.13\,\mathrm{kbp\,s^{-1}}$.

DIFFUSIVITY OF TRANSIENTLY EXTRUDED SYSTEMS

Despite being only partially extruded the average mean squared displacement for the center of mass of the polymers (Fig. S7) shows the loss of subdiffusive behaviour at early times, whilst displaying also the LEF-dependent increase in diffusivity already discussed in the main text. However, the value of partially extruded-related MSDs is found to be always smaller than the corresponding fully-extruded MSDs.

[1] Kurt Kremer and Gary S. Grest. Dynamics of entangled linear polymer melts: A molecular-dynamics simulation. *The Journal of Chemical Physics*, 92(8):5057–5086, 1990.

[2] Steve Plimpton. Fast Parallel Algorithms for Short-Range Molecular Dynamics. *J. Comp. Phys.*, 117(1):1–19, 1995.

[3] Geoffrey Fudenberg, Maxim Imakaev, Carolyn Lu, Anton Goloborodko, Nezar Abdennur, and Leonid A. Mirny. Formation of Chromosomal Domains by Loop Extrusion. *Cell Reports*, 15(9):2038–2049, May 2016.

[4] Anton Goloborodko, John F. Marko, and Leonid A. Mirny. Chromosome Compaction by Active Loop Extrusion. *Biophysical Journal*, 110(10):2162–2168, May 2016.

[5] Enzo Orlandini, Davide Marenduzzo, and Davide Michieletto. Synergy of Topoisomerase and Structural-Maintenance-of Chromosomes Proteins Creates a Universal Pathway to Simplify Genome Topology. In *Proceedings of the National Academy of Science USA*, volume 116, page 8149, 2019.

[6] A. P. Thompson, H. M. Aktulga, R. Berger, D. S. Bolintineanu, W. M. Brown, P. S. Crozier, P. J. in 't Veld, A. Kohlmeyer, S. G. Moore, T. D. Nguyen, R. Shan, M. J. Stevens, J. Tranchida, C. Trott, and S. J. Plimpton. LAMMPS - a flexible simulation tool for particle-based materials modeling at the atomic, meso, and continuum scales. *Comp. Phys. Comm.*, 271:108171, 2022.

[7] Jonathan D Halverson, Won Bo Lee, Gary S Grest, Alexander Y Grosberg, and Kurt Kremer. Molecular dynamics simulation study of nonconcatenated ring polymers in a melt. II. Dynamics. *The Journal of chemical physics*, 134(20):204905, may 2011.

[8] Ralf Everaers, Sathish K. Sukumaran, Gary S. Grest, Carsten Svaneborg, Arvind Sivasubramanian, and Kurt Kremer. Rheology and Microscopic Topology of Entangled Polymeric Liquids. *Science*, 303(5659):823–826, February 2004.

[9] Won Bo Lee and Kurt Kremer. Entangled Polymer Melts: Relation between Plateau Modulus and Stress Autocorrelation Function. *Macromolecules*, 42(16):6270–6276, aug 2009.

[10] Jorge Ramírez, Sathish K. Sukumaran, Bart Vorselaars, and Alexei E. Likhtman. Efficient on the fly calculation of time correlation functions in computer simulations. *The Journal of Chemical Physics*, 133(15), October 2010.

[11] Mahipal Ganji, Indra A Shaltiel, Shveta Bisht, Eugene Kim, Ana Kalichava, Christian H Haering, and Cees Dekker. Real-time imaging of DNA loop extrusion by condensin. *Science*, 360(6384):102–105, 2018.